J. Mod. Power Syst. Clean Energy (2016) 4(4):690–701
DOI 10.1007/s40565-016-0227-2

Optimal power flow calculation in AC/DC hybrid power system based on adaptive simplified human learning optimization algorithm

Jia CAO[1], Zheng YAN[1], Xiaoyuan XU[1], Guangyu HE[1], Shaowei HUANG[2]

Abstract This paper employs an efficacious analytical tool, adaptive simplified human learning optimization (ASHLO) algorithm, to solve optimal power flow (OPF) problem in AC/DC hybrid power system, considering valve-point loading effects of generators, carbon tax, and prohibited operating zones of generators, respectively. ASHLO algorithm, involves random learning operator, individual learning operator, social learning operator and adaptive strategies. To compare and analyze the computation performance of the ASHLO method, the proposed ASHLO method and other heuristic intelligent optimization methods are employed to solve OPF problem on the modified IEEE 30-bus and 118-bus AC/DC hybrid test system. Numerical results indicate that the ASHLO method has good convergent property and robustness. Meanwhile, the impacts of wind speeds and locations of HVDC transmission line integrated into the AC network on the OPF results are systematically analyzed.

Keywords Adaptive simplified human learning optimization algorithm, Optimal power flow, AC/DC hybrid power system, Valve-point loading effects of generators, Carbon tax, Prohibited operating zones

CrossCheck date: 4 July 2016

Received: 13 November 2015 / Accepted: 4 July 2016 / Published online: 17 September 2016

✉ Jia CAO
caojia2013@sjtu.edu.cn

Zheng YAN
yanz@sjtu.edu.cn

Xiaoyuan XU
xuxiaoyuansjtu@gmail.com

Guangyu HE
heguangyu@beepower.cn

Shaowei HUANG
hsw02@mail.tsinghua.edu.cn

[1] The Ministry of Education Key Laboratory of Control of Power Transmission and Conversion, Department of Electrical Engineering, Shanghai Jiao Tong University, Shanghai 200240, China

[2] State Key Laboratory of Power Systems, Department of Electrical Engineering, Tsinghua University, Beijing 100084, China

1 Introduction

With the increasingly wide use of high-voltage direct current (HVDC) transmission line as well as large scale sustainable energy integration, the operation of modern power system becomes as more complex and changeable than ever before. Therefore, how to analyze the impacts of HVDC transmission line and sustainable energy integration on the optimal power flow (OPF) results has been drawn great attention.

Currently, there are a lot of researchers and scholars to study the OPF problem considering HVDC transmission line [1–3] or sustainable energy integration [4–6], separately. The AC/DC OPF problem with voltage source converter based multi-terminal DC networks is proposed in [1], which is to minimize the transmission loss of the whole AC/DC network with two different voltage source converter control strategies considered. In [2], based on information gap decision theory, the OPF model of AC/DC hybrid system with high penetration of offshore wind farms is developed. A method for solving the OPF and security constrained OPF problem in AC/DC hybrid system is proposed in [3]. By using improved levenberg-marquardt method [4] and interior point method [5], the OPF problem including wind farm

STATE GRID
STATE GRID ELECTRIC POWER RESEARCH INSTITUTE

integration is solved. And, variational key issues, wind speed, wind turbine number and wind power penetration level, to influence the static performance of power system are analyzed in [4]. To take the random characteristic of wind speed into account, a dividing-stage strategy and a multi-period dynamic OPF model are presented in [6].

However, it is difficult to find the literatures about OPF problem considering both HVDC transmission line and sustainable energy integration simultaneously. Besides, the OPF model becomes more and more complex due to taking the practical operation condition into account, such as prohibited operating zones [7, 8], valve-point loading effects of generators [9–14] and carbon tax [15–17]. Under the complex circumstance, the objective function in the constructed OPF model becomes as discontinuous, non-convex and non-differentiable. Therefore, the derivative-based mathematical optimization method [4, 5] can not be employed to solve the OPF problem. To find a method with good convergent property and robustness to solve OPF problem considering those critical conditions above is the primary job of this paper.

Luckily, an adaptive simplified human learning optimization (ASHLO) method emerges [18], which updates new solutions and searches for the optimal solution by mimicking the human learning process. The random learning operator, individual learning operator, social learning operator and adaptive strategies are involved in the ASHLO method. The excellence of global search ability and the robustness for various problems [18] are the primary characteristics of the ASHLO method. Therefore, application of ASHLO method to solve OPF problem in AC/DC hybrid power system including wind farms integration is main contribution of this paper. Meanwhile, comparison and analysis of the computation performances of the ASHLO method compared to other heuristic intelligent optimization method, e.g., genetic algorithm (GA), discrete binary particle swarm optimization (DBPSO) method, binary harmony search (BHS) algorithm and simple HLO method, are made in this paper. The impacts of wind speeds and locations of HVDC transmission line into the power system on the OPF results are also systematically analyzed.

This paper firstly presents the OPF model of AC/DC hybrid power system with wind farms integration in Section 2, considering prohibited operating zones, valve-point loading effects of generators and carbon tax. Section 3 gives a brief description of the ASHLO method, involving random learning operator, individual learning operator, social learning operator and adaptive strategies. The proposed ASHLO method to solve AC/DC OPF problem on the modified IEEE 30-busand 118-bus test system, and the analysis of the impacts of wind speeds and locations of HVDC line into the power system on the OPF results are reported in Section 4, followed by the conclusions in Section 5.

2 OPF model of AC/DC hybrid power system with wind farms integration

2.1 Objective function of OPF problem

Taking minimum fuel costs of the conventional generators as the expected target as well as taking the valve-point loading effects of generators, prohibited operating zones and carbon tax into account, the objective function of OPF model can be described in (1) [8, 15],

$$\min \sum_{i=1}^{N_G} \left\{ \begin{array}{l} a_{2i}P_{Gi}^2 + a_{1i}P_{Gi} + a_{0i} + \left| e_i \sin[f_i(P_{Gi}^{\min} - P_{Gi})] \right| \\ + P_i(s_i P_{Gi}^2 + r_i P_{Gi} + q_i) \end{array} \right\} \tag{1}$$

where N_G is the set of conventional generators; a_{2i}, a_{1i}, a_{0i} are the fuel cost coefficients of generators; e_i, f_i are the fuel consumption coefficients considering valve-point loading effects of generators; p_i is the price of carbon emission; s_i, r_i, q_i are the carbon emission coefficients of generators; P_{Gi} is the real power of the i^{th} generator; $P_{Gi}^{\min}$ is the lower bound of the real power of the i^{th} generator, respectively. Meanwhile, the control variables, output of the generators, become discontinuous due to considering the prohibited operating zones [8], which are shown in (2):

$$P_{Gi} \in [P_{Gi}^{\min}, P_{Gi,1}^{l}] \cup [P_{Gi,1}^{u}, P_{Gi,2}^{l}] \cup \cdots \cup [P_{Gi,K}^{u}, P_{Gi}^{\max}] \tag{2}$$

where $P_{Gi}^{\max}$ is the upper bound of the real power of the i^{th} generator; $P_{Gi,j}^{u}$ and $P_{Gi,j+1}^{l}$ are the upper and lower bound of the j^{th} and $j+1^{th}$ prohibited operating zones of the i^{th} generator, respectively.

2.2 Equality constraints of OPF problem

The wind farm is assumed to connect with node i. The double-fed induction generator (DFIG) is applied to the wind turbine generator, and the consumption of reactive power can be compensated by the controller. Therefore, the control mode with the constant power factor of wind turbine generator can remain unchanged [19–21]. In order to avoid the influence of reactive power consumption of wind turbines on OPF results, the power factor is maintained at 1.0 in this paper, which means that the reactive power output of wind farm can be as 0 approximately. P_{wi} is the active powers provided by wind generators. The relationship between P_{wi} and wind speed V is shown in Fig. 1, where V_{ci}, V_r and V_{co} are the cut-in wind speeds, rated wind speeds and cut-out wind speeds, P_r is the rated active power of wind generators, respectively.

For the AC node, the AC power flow equations are written as:

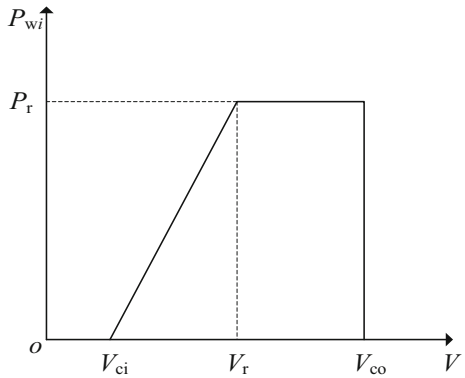

Fig. 1 Wind speed and active power curve of wind generators

$$\begin{cases} \Delta P_i = P_{Gi} + P_{wi} - P_{Di} - U_i \sum\limits_{j\in i} U_j(G_{ij}\cos\theta_{ij} + B_{ij}\sin\theta_{ij}) = 0 \\ \Delta Q_i = Q_{Gi} - Q_{Di} - U_i \sum\limits_{j\in i} U_j(G_{ij}\sin\theta_{ij} - B_{ij}\cos\theta_{ij}) = 0 \end{cases} \tag{3}$$

where Q_{Gi} is the reactive power by generator; P_{Di}, Q_{Di} are real and reactive load; U_i is the amplitude of node voltage; G_{ij}, B_{ij} are conductance and susceptance between node i and j; θ_{ij} is the difference of phase angle of node voltage between node i and j, respectively.

For the DC node, the DC transmission power should be added into the power flow equations, and the power flow equations should be modified as:

$$\begin{cases} \Delta P_i = P_{Gi} - P_{Di} - U_i \sum\limits_{j\in i} U_j(G_{ij}\cos\theta_{ij} + B_{ij}\sin\theta_{ij}) \\ \qquad - U_{dk} I_{dk}\,\mathrm{sign}(i) + P_{wi} = 0 \\ \Delta Q_i = Q_{Gi} - Q_{Di} - U_i \sum\limits_{j\in i} U_j(G_{ij}\sin\theta_{ij} - B_{ij}\cos\theta_{ij}) \\ \qquad - U_{dk} I_{dk}\tan\phi_k = 0 \end{cases} \tag{4}$$

where I_{dk} is the DC current; U_{dk} is the DC voltage; ϕ_k is the power factor angle; $\mathrm{sign}(i) = 1$ for the rectifier, $\mathrm{sign}(i) = -1$ for the inverter, respectively.

Meanwhile, the DC system includes converter voltage equations, Δd_{1k} and Δd_{2k}, DC network equations Δd_{3k} and control equations Δd_{4k} and Δd_{5k}, which are expressed in (5) [22–24]:

$$\begin{cases} \Delta d_{1k} = U_{dk} - k_{Tk} U_i \cos\theta_{dk} + X_{ck} I_{dk} \\ \Delta d_{2k} = U_{dk} - k_\gamma k_{Tk} U_i \cos\phi_k \\ \Delta d_{3k} = \mathrm{sign}(k) I_{dk} - \sum\limits_{j=1}^{n_c} g_{dkj} U_{dj} \qquad k = 1, 2, \ldots, n_c \\ \Delta d_{4k} = d_{4k}(I_{dk}, U_{dk}, \cos\theta_{dk}, k_{Tk}) \\ \Delta d_{5k} = d_{5k}(I_{dk}, U_{dk}, \cos\theta_{dk}, k_{Tk}) \end{cases} \tag{5}$$

where n_c is the number of converters; k_{Tk} is the ratio of converter transformer; X_{ck} is commutation reactance; θ_{dk} is the trigger angle α_r for the rectifier; θ_{dk} is the extinction angle γ_i for the inverter; k_γ is the constant [24]; g_{dkj} is the elements of node conductance matrix in the DC network after eliminating the contact node.

2.3 Inequality constraints of OPF problem

The inequality constraints of the OPF problem contain two categories, the security constraints for AC part and

$$\begin{cases} P_{Gi}^{\min} \le P_{Gi} \le P_{Gi}^{\max} & i \in N_G \\ Q_{Gi}^{\min} \le Q_{Gi} \le Q_{Gi}^{\max} & i \in N_G \\ t_{ij}^{\min} \le t_{ij} \le t_{ij}^{\max} & (i,j) \in N_T \\ U_i^{\min} \le U_i \le U_i^{\max} & i \in \{1, 2, \ldots, n\} \\ 0 \le I_{ij}^2 \le (I_{ij}^2)^{\max} & (i,j) \in N_L \\ 0 \le Q_{ci} \le Q_{ci}^{\max} & i \in N_c \\ U_{dk}^{\min} \le U_{dk} \le U_{dk}^{\max} & k \in \{1, 2, \ldots, n_c\} \\ I_{dk}^{\min} \le I_{dk} \le I_{dk}^{\max} & k \in \{1, 2, \ldots, n_c\} \\ k_{Tk}^{\min} \le k_{Tk} \le k_{Tk}^{\max} & k \in \{1, 2, \ldots, n_c\} \\ \theta_{dk}^{\min} \le \theta_{dk} \le \theta_{dk}^{\max} & k \in \{1, 2, \ldots, n_c\} \end{cases} \tag{6}$$

that for DC part. In short, the whole security constraints can be written as in (6), where $P_{Gi}^{\max}$, $Q_{Gi}^{\max}$, $t_{ij}^{\max}$, $U_i^{\max}$, $(I_{ij}^2)^{\max}$, $Q_{ci}^{\max}$, $U_{dk}^{\max}$, $I_{dk}^{\max}$, $k_{Tk}^{\max}$, $\theta_{dk}^{\max}$ are the upper bound of the real power, reactive power of generator, ratio of transformer, amplitude of node voltage, line currents, shunt capacitor, DC voltage, DC current, ratio of converter transformer, trigger angle or extinction angle, respectively; N_T, N_L, N_c are the set of the transformer, the restricted line and shunt capacitors, respectively. Besides, line current of branch $i - j$ can be expressed as in (7):

$$\begin{aligned} I_{ij}^2 = (G_{ij}^2 + B_{ij}^2)[&(U_i\cos\theta_i - U_j\cos\theta_j)^2 \\ &+ (U_i\sin\theta_i - U_j\sin\theta_j)^2] \end{aligned} \tag{7}$$

Hence, the OPF calculation in AC/DC hybrid power system can be simplified as the nonlinear optimization problem in (8):

$$\begin{cases} \min \quad zf(\boldsymbol{x}) \\ s.t. \quad \boldsymbol{g}(\boldsymbol{x}) = 0 \\ \qquad \boldsymbol{h}(\boldsymbol{x}) \ge 0 \end{cases} \tag{8}$$

where $\boldsymbol{x} = [\boldsymbol{P}_G^T, \boldsymbol{Q}_G^T, \boldsymbol{t}^T, \boldsymbol{U}^T, \boldsymbol{Q}_c^T, (\boldsymbol{I}_{ij}^2)^T, \boldsymbol{U}_{dk}^T, \boldsymbol{I}_{dk}^T, \boldsymbol{k}_{Tk}^T, \boldsymbol{\theta}_{dk}^T] \in R^n$ is the vector of control variables and state variables; $f(\boldsymbol{x})$ is the objective function; $\boldsymbol{g}(\boldsymbol{x})$ is the equality constraints, including AC node power flow equations, DC node power flow equations, and DC system equations; $\boldsymbol{h}(\boldsymbol{x})$ is the inequality constraints, including AC security constraints and DC security constraints, respectively.

3 Adaptive simplified human learning optimization algorithm

Adaptive simplified human learning optimization(ASHLO) algorithm involves the random learning operator, individual learning operator, social learning operator [25–27], and adaptive strategies [18], which are mimicking human learning process, to find the optimal solution of the optimization problem. The remarkable feature of the ASHLO method is not easy falling into the local optima.

Suppose that the i^{th} solution, based on decimal base, of the optimization problem is composed of N elements in (9):

$$\boldsymbol{x}_i^{\text{decimal}} = [x_{i,1}^{\text{d}}, x_{i,2}^{\text{d}}, \ldots, x_{i,N}^{\text{d}}] \tag{9}$$

Then, by using the binary encoding technique, the solution in (9) can be extended as in (10), where each M binary bits in (10) represents an element in (9), and the relationship is $P = N \cdot M$. Besides, the transformation relationship between one element $x_{i,j}^{\text{d}}$ in (9) and M bits in (10) can be expressed in (11):

$$\boldsymbol{x}_i^{\text{binary}} = [x_{i,1}^{\text{b}}, \ldots, x_{i,M}^{\text{b}}, x_{i,M+1}^{\text{b}}, \ldots, x_{i,2M}^{\text{b}}, \ldots, x_{i,(N-1)\cdot M+1}^{\text{b}}, \ldots, x_{i,P}^{\text{b}}] \tag{10}$$

$$x_{i,j}^{\text{d}} = x_{i,j}^{\text{d,min}} + \frac{(x_{i,j}^{\text{d,max}} - x_{i,j}^{\text{d,min}})}{2^M - 1} \left\{ \sum_{l=1}^{M} \left(x_{i,l}^{\text{b}} 2^{(M-l)} \right) \right\} \tag{11}$$

where $x_{i,j}^{\text{d,min}}$ and $x_{i,j}^{\text{d,max}}$ are the lower and upper bound of the jth element in (9).

By initializing all the individuals, the population of ASHLO method is obtained in (12), where O is the number of population; P is the dimension of solution encoded by binary encoding technique; $\boldsymbol{x}_i$ is the i^{th} individual, respectively.

$$\boldsymbol{X} = \begin{bmatrix} \boldsymbol{x}_1 \\ \boldsymbol{x}_2 \\ \vdots \\ \boldsymbol{x}_i \\ \vdots \\ \boldsymbol{x}_O \end{bmatrix} = \begin{bmatrix} x_{11} & x_{12} & \cdots & x_{1j} & \cdots & x_{1P} \\ x_{21} & x_{22} & \cdots & x_{2j} & \cdots & x_{2P} \\ \vdots & \vdots & & \vdots & & \vdots \\ x_{i1} & x_{i2} & \cdots & x_{ij} & \cdots & x_{iP} \\ \vdots & \vdots & & \vdots & & \vdots \\ x_{O1} & x_{O2} & \cdots & x_{Oj} & \cdots & x_{OP} \end{bmatrix} \tag{12}$$
$$x_{ij} \in \{0, 1\},\ 1 \le i \le O,\ 1 \le j \le P$$

3.1 Random learning operator

Random learning is defined as the process that individuals can explore new strategies randomly to escape from the local optima. New individuals can be generated in (13) when ASHLO method performs random learning operator.

$$x_{ij} = Rand(0, 1) = \begin{cases} 0, & 0 \le rand() < 0.5 \\ 1, & 0.5 \le rand() \le 1 \end{cases} \tag{13}$$

where $rand()$ is a stochastic number between 0 and 1.

3.2 Individual learning operator

$$\boldsymbol{B}_{\text{IKD}_i} = \begin{bmatrix} \boldsymbol{b}_{i1} \\ \boldsymbol{b}_{i2} \\ \vdots \\ \boldsymbol{b}_{ir} \\ \vdots \\ \boldsymbol{b}_{iL} \end{bmatrix} = \begin{bmatrix} b_{i1,1} & b_{i1,2} & \cdots & b_{i1,j} & \cdots & b_{i1,P} \\ b_{i2,1} & b_{i2,2} & \cdots & b_{i2,j} & \cdots & b_{i2,P} \\ \vdots & \vdots & & \vdots & & \vdots \\ b_{ir,1} & b_{ir,2} & \cdots & b_{ir,j} & \cdots & b_{ir,P} \\ \vdots & \vdots & & \vdots & & \vdots \\ b_{iL,1} & b_{iL,2} & \cdots & b_{iL,j} & \cdots & b_{iL,P} \end{bmatrix} \tag{14}$$
$$1 \le i \le O,\ 1 \le r \le L,\ 1 \le j \le P,\ b_{ir,j} \in \{0, 1\}$$

Individuals learn to search for the optima by the individual learning operator based on their individual knowledge database ($\boldsymbol{B}_{\text{IKD}}$), which is used to store personal best experience, where $\boldsymbol{B}_{\text{IKD}_i}$ in (14) is the individual knowledge database of person i, $\boldsymbol{b}_{ir}$ is the r^{th} best solution of person i, L is the size of the $\boldsymbol{B}_{\text{IKD}_i}$. New individuals can be updated in (14) based on the knowledge in the $\boldsymbol{B}_{\text{IKD}}$ when ASHLO method performs individual learning.

$$x_{ij} = b_{ir,j} \tag{15}$$

3.3 Social learning operator

Like individual learning operator, a social knowledge database ($\boldsymbol{D}_{\text{SKD}}$) is also constructed in (16) to store the best individual of the population. Therefore, social learning is defined as the process that all the individuals learn from the best individual of the population.

$$\boldsymbol{D}_{\text{SKD}} = \begin{bmatrix} \boldsymbol{d}_1 \\ \boldsymbol{d}_2 \\ \vdots \\ \boldsymbol{d}_s \\ \vdots \\ \boldsymbol{d}_T \end{bmatrix} = \begin{bmatrix} d_{1,1} & d_{1,2} & \cdots & d_{1,j} & \cdots & d_{1,P} \\ d_{2,1} & d_{2,2} & \cdots & d_{2,j} & \cdots & d_{2,P} \\ \vdots & \vdots & & \vdots & & \vdots \\ d_{s,1} & d_{s,2} & \cdots & d_{s,j} & \cdots & d_{s,P} \\ \vdots & \vdots & & \vdots & & \vdots \\ d_{T,1} & d_{T,2} & \cdots & d_{T,j} & \cdots & d_{T,P} \end{bmatrix} \tag{16}$$
$$1 \le s \le T,\ 1 \le j \le P,\ 1 \le T \le O,\ d_{s,j} \in \{0, 1\}$$

where T is the size of the $\boldsymbol{D}_{\text{SKD}}$; $\boldsymbol{d}_s$ is the sth best individual of the population in the $\boldsymbol{D}_{\text{SKD}}$. Based on the knowledge in the $\boldsymbol{D}_{\text{SKD}}$, new individuals can be updated in (17) when ASHLO method performs social learning.

$$x_{ij} = d_{s,j} \tag{17}$$

3.4 Adaptive strategies

According to the random learning operator, individual learning operator, and social learning operator, new individuals can be updated in (18) iteratively based on the experience knowledge stored in the $\boldsymbol{B}_{\mathrm{IKD}}$ and $\boldsymbol{D}_{\mathrm{SKD}}$.

$$x_{ij} = \begin{cases} rand(0,1) & 0 \le rand(\ ) \le p_r \\ b_{ir,j} & p_r < rand(\ ) \le p_i \\ d_{s,j} & p_i < rand(\ ) \le 1 \end{cases} \tag{18}$$

where parameters p_r, $p_i - p_r$, $1 - p_i$ are the probabilities to perform random learning, individual learning, and social learning, respectively. To avoid falling into the local optima and improve the robustness of the ASHLO method, adaptive strategies are proposed in [18] to improve the search efficiency and relieve the effort of the parameters setting, since p_r and $p_i$influence the computation performance of the algorithm. Therefore, the adaptive strategies put forward in (19), which involves updating p_r and p_i adaptively.

$$\begin{cases} p_r = p_r^{\max} - \dfrac{p_r^{\max} - p_r^{\min}}{N_{\max}^{\mathrm{Ite}}} N_i^{\mathrm{Ite}} \\ p_i = p_i^{\min} + \dfrac{p_i^{\max} - p_i^{\min}}{N_{\max}^{\mathrm{Ite}}} N_i^{\mathrm{Ite}} \end{cases} \tag{19}$$

where N_i^{Ite} and $N_{\max}^{\mathrm{Ite}}$ are the current iteration number and maximum iteration number; $p_r^{\min}$ and $p_i^{\min}$ are the minimum value of p_r and p_i; $p_r^{\max}$ and $p_i^{\max}$ are the maximum value of p_r and p_i, respectively. Therefore, during the early stage of the iteration process, the individuals will move in the direction towards the optimal individual of the initial population, which can speed up the convergent speed. Meanwhile, the large probability p_r to perform random learning at the early stage of the iteration process is also to keep population diversity and avoid falling into the local optima. In contrast, during the end of stage of the iteration process, the individuals will primarily move in the direction towards the optima of each individual, which can effectively obtain stable optimal solution.

In short, according to the description of the ASHLO method, the flowchart of the ASHLO method to solve OPF problem in AC/DC hybrid power system is given in Fig. 2.

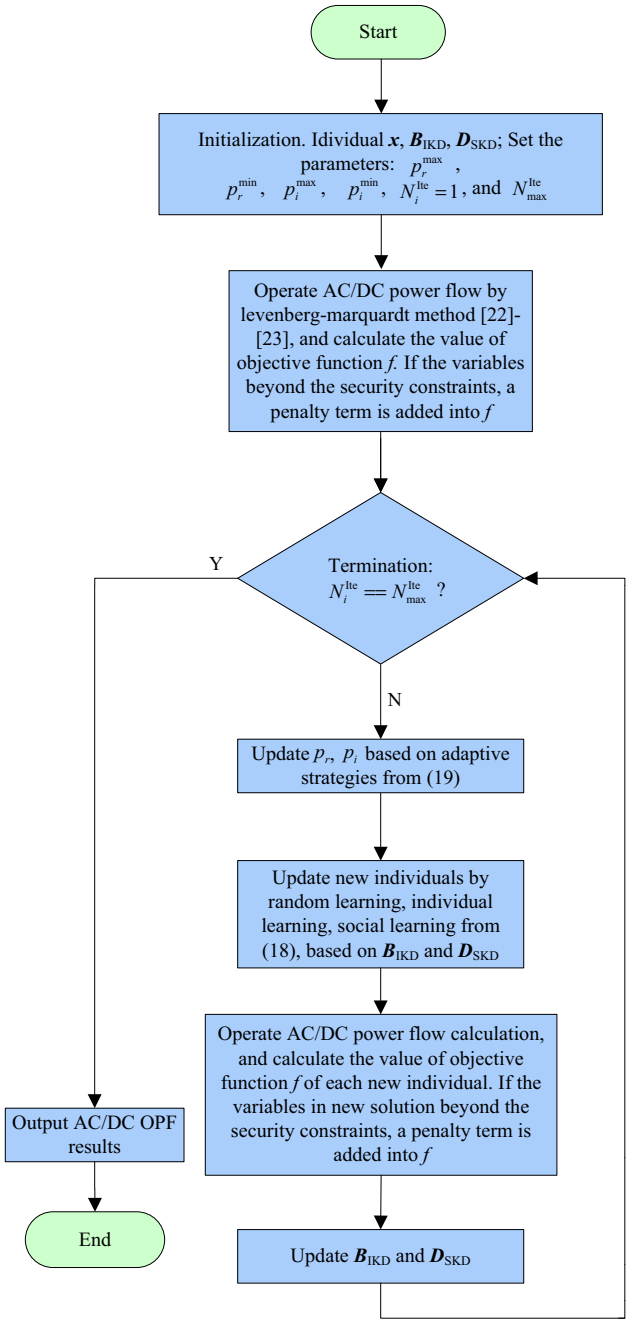

Fig. 2 Flow chart of the ASHLO method to solve AC/DC OPF problem

4 Numerical results and discussion

The AC/DC OPF problem considering valve-point loading effects of generators, prohibited operating zones, and carbon tax, is tested on the modified IEEE 30-bus[4] and IEEE 118-bus [22, 23] AC/DC hybrid test system. The test is operated on an advanced micro devices (ADM) 3.20 GHz with 4.00 GB of RAM. Without specification, all data are taken as per-unit value and base value is 100 MVA. A computer program is implemented in MATLAB to solve the AC/DC OPF problem.

4.1 ModifiedIEEE 30-bus AC/DC hybrid test system

The modified IEEE 30-bus AC/DC hybrid test system derives from the IEEE 30-bus system [4], adding one DC transmission line into AC network connecting node 10 and

23. The converter connected to node 10 is rectifier and to 23 is inverter. The corresponding parameters and control mode of HVDC transmission line are given in Table 1 [22, 23]. Besides, the upper bound of the line currents $(I_{ij}^2)^{\max}$ is set three times as large as that in the original IEEE 30-bus test system due to adding one HVDC transmission line.

Meanwhile, the parameters in ASHLO method are set as the number of population $O = 50$, the dimension of solution based on binary encoding $P = 300$, including 15 control variables and 20 binary bits for each variable due to the coupling relationship between AC variables and DC variables as well as the specified control mode for HVDC line, the probability $p_r^{\max} = 10/P$, $p_r^{\min} = 1/P$, $p_i^{\max} = 0.9 + 1/P$, $p_i^{\min} = 0.8 + 1/P$ [18], the penalty multiplier $\lambda = 10000$, respectively. To test the computation performance of the proposed ASHLO method, the genetic algorithm (GA), discrete binary particle swarm optimization method (DBPSO), human learning optimization method without adaptive strategies (HLO), and binary harmony search algorithm (BHS) are also employed to solve AC/DC OPF problem. In order to simplify the solution procedure, the value of r and s in (19) is identical to 1. Table 2 gives the fuel cost coefficients and the coefficients of valve-point loading effects of generators. Table 3 and Table 4 give the carbon tax coefficients and upper and lower bound of the real and reactive power of generators.

To begin with, we do the research on the impacts of maximal iteration number, $N_{\max}^{\text{Ite}}$, on the OPF results obtained by ASHLO method, since the probabilities p_r and p_i are associated with $N_{\max}^{\text{Ite}}$. At this time, no wind farms are assumed to integrate with this hybrid power system, and fifty times independent repeated experiments are carried out by ASHLO method under different $N_{\max}^{\text{Ite}}$. The relationship between $N_{\max}^{\text{Ite}}$ and the objective function obtained by ASHLO method is given in Table 5, including the minimum, maximum, mean, and standard deviation of the objective function. From the Table 5, the impacts of $N_{\max}^{\text{Ite}}$ on the OPF results exist. Within a certain range, the more stable solutions can be obtained with the increasing of $N_{\max}^{\text{Ite}}$. However, the stability of the ASHLO method will be deteriorated if the $N_{\max}^{\text{Ite}}$ is beyond 200. So, we take $N_{\max}^{\text{Ite}} = 200$ as the parameter in the ASHLO method.

Meanwhile, to compare the computation performance of the ASHLO method, fifty times independent repeated experiments are also carried out by HLO method, GA method, DBPSO method, and BHS method, respectively. Figure 3 shows the objective function of different methods under different run times, and Table 6 summarizes the

Table 1 Parameter and control mode of HVDC line

HVDC line		Line parameters	Control mode
Rectifier	Inverter		
10	23	$X_{c1} = X_{c2}$=0.013 $R = 0.0388$	Rectifier: α_r, P_{dr} Inverter: γ_i, U_{di}

Table 2 Cost coefficients of fuel and valve-point loading effects of generators

Generator number	α_{2i}	α_{1i}	α_{0i}	e_i	f_i
1	384.32	2000	0	1800	3.7
2	2500	2000	0	1600	3.8
3	100	4000	0	1400	4.0
4	100	4000	0	1200	4.5
5	100	4000	0	1300	4.2
6	100	4000	0	1350	4.1

Table 3 Carbon tax coefficients

Generator number	p_i	s_i	r_i	q_i
1	320	0.004	0.25	0
2	320	0.005	0.25	0
3	320	0.004	0.25	0
4	185	0.500	4.0	0
5	185	0.500	4.0	0
6	285	0.010	2.0	0

Table 4 Upper and lower bound of the real and reactive power of generators

Generator number	$P^{\max}$	$P^{\min}$	$Q^{\max}$	$Q^{\min}$	Prohibited operating zones
1	3.602	0	0.1	0	[1.65, 2.05]
2	1.4	0	0.5	−0.4	[0.65, 0.85]
3	1.0	0	0.4	−0.4	[0.45, 0.65]
4	1.0	0	0.4	−0.1	[0.45, 0.65]
5	1.0	0	0.24	−0.06	[0.45, 0.65]
6	1.0	0	0.24	−0.06	[0.45, 0.65]

Table 5 Relationship between $N_{\max}^{\text{Ite}}$ and objective function obtained by ASHLO method

$N_{\max}^{\text{Ite}}$	$f^{\min}$	$f^{\max}$	f^{mean}	$f^{\text{deviation}}$
50	12710	25046	17928	4461
100	11945	23878	16364	4359
200	11471	23738	14773	4216
300	11484	23346	14405	4332

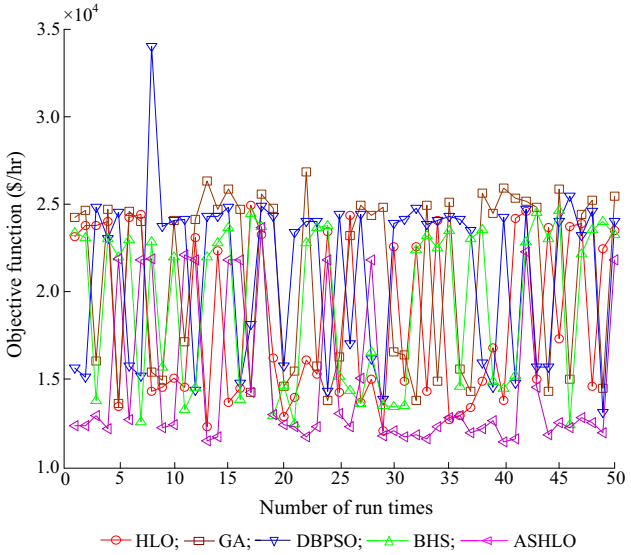

Fig. 3 Objective function of different methods under different run times

Table 6 Results of objective function of different methods

Method	$f^{\min}$	$f^{\max}$	f^{mean}	$f^{\text{deviation}}$
HLO	12124	24999	18496	4765
GA	13678	26891	21076	4938
DBPSO	13175	34025	21244	4718
BHS	12483	24690	19406	4631
ASHLO	11471	23738	14773	4216

minimum, maximum, mean, and standard deviation of the objective function by different methods during the fifty times independent repeated experiments. It can be observed from the Table 6 that, all the computation performances, including minimum, maximum, mean, and standard deviation of objective function, obtained by ASHLO method are less than that by other methods. It is noted that the maximal objective function obtained by DBPSO method reaches 34025 $/hr, which is caused by one of the control variables or state variables in the solution beyond the constraints and adding additional penalty term, $\lambda = 10000$. Moreover, from the Fig. 3, compared to other methods, the ASHLO method also gets the slightest fluctuation of objective function, which implies that the ASHLO method has good convergent property and robustness.

Furthermore, based on the good computation performances of the ASHLO method, we can take wind farms to integrate with this AC/DC hybrid test system, and research the impacts of wind speeds on the OPF results. There are assumed 20 identical wind generators in each wind farm, and each wind generator has the nominal capacities equal to 600 kW. The equivalent wind farms are connected to nodes 7, 17, 21, and 30 of this modified IEEE 30-bus AC/DC hybrid test system. The identical cut-in wind speed, cut-out wind speed and rated wind speed of wind farm are set as 3, 20, 13.5 m/s, respectively. Figs. 4, 5, 6, 7, 8, 9 and 10 describe the corresponding solutions under different wind speeds, including objective function, real and reactive power of generators, amplitude of AC node voltage, ratio of transformers and shunt capacitors, and DC variables, respectively.

It can be seen from the Fig. 4 that the total cost is decreased with the increasing of wind speed V, which is from 11471 $/hr at wind speed $V = 0$ to 9061.6 $/hr at rated wind speed V_r. That demonstrates the wind farm integration plays a positive role in reducing the total cost. Compared to the total cost, the valve-point cost is increased with the increasing of wind speed and decreased

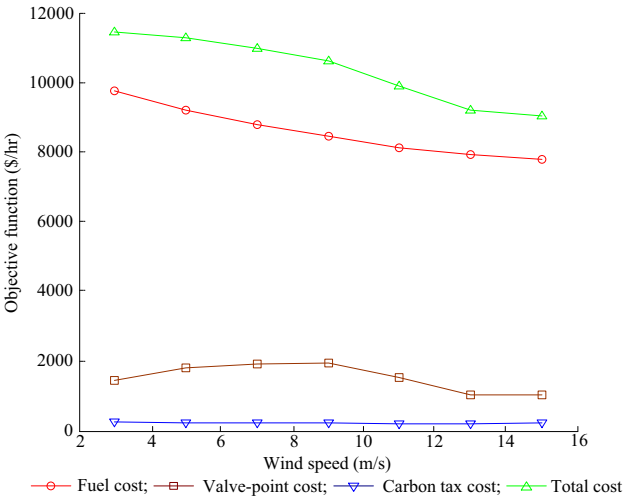

Fig. 4 Objective function under different wind speeds

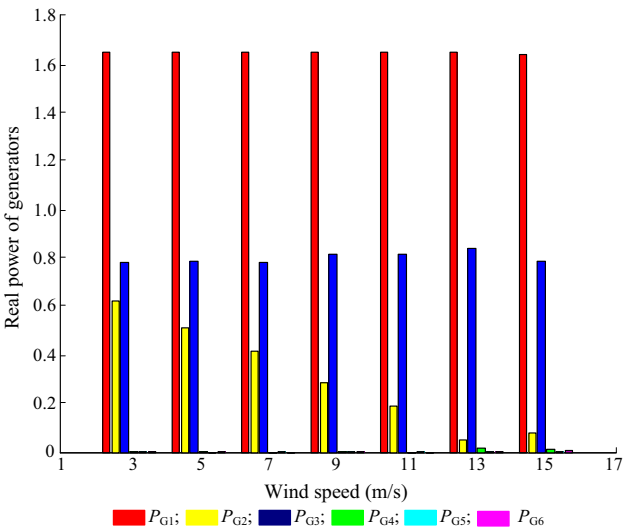

Fig. 5 Real power of generators under different wind speeds

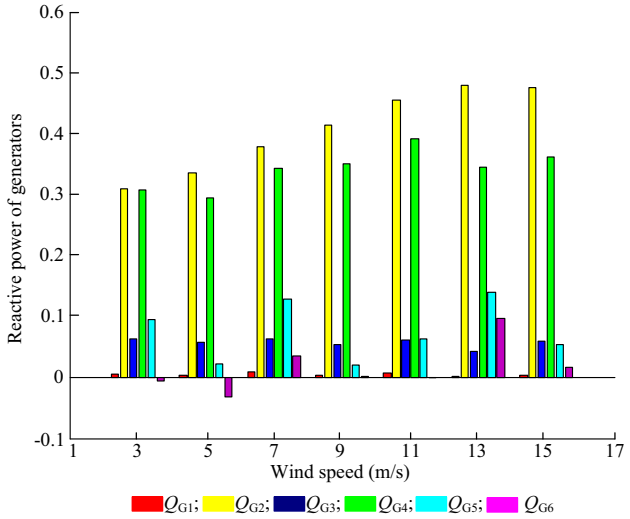

Fig. 6 Reactive power of generators under different wind speeds

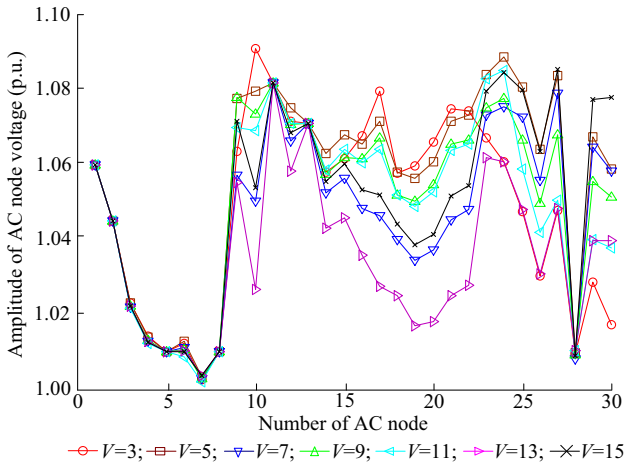

Fig. 7 Amplitude of AC node voltage under different wind speeds

afterwards, which also indicates the introduction of wind farm will not always decrease the valve-point cost. Because, according to (1), the valve-point cost is determined by its function property.

From the Fig. 5, except the generator 2, there are no obvious change in the real power of other generators, which implies the decreasing of total cost is mainly caused by reducing output of the generator 2 with the increasing of wind speed. Because, with the wind farm integration, it is priority to reduce the output of generator 2 from the economic point of view due to its large power generation cost coefficient. From the Fig. 6, different reactive power of generators under variational wind speeds are obtained, which are mainly used to the consumption of the reactive load and the converter in this AC/DC hybrid system. Meanwhile, it can be seen from the Figs. 7–8 that, the amplitude of AC node voltage varies from the different

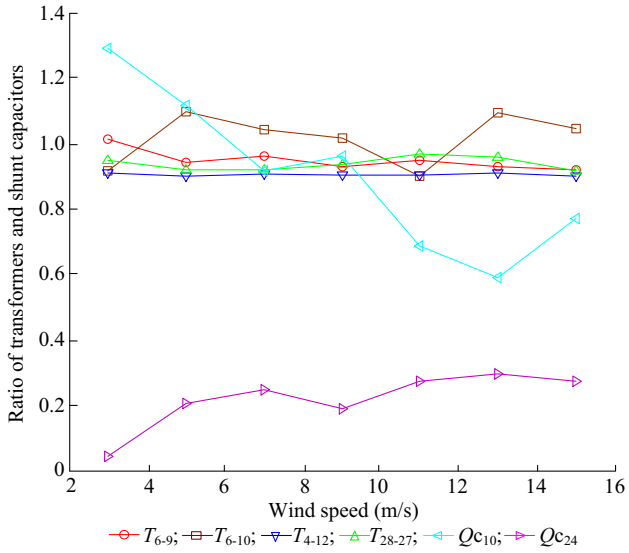

Fig. 8 Ratio of transformers and shunt capacitors under different wind speeds

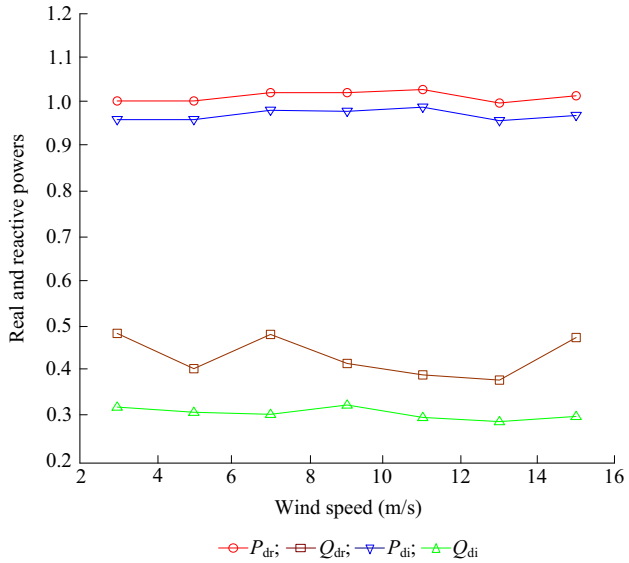

Fig. 9 Real and reactive powers of rectifier and inverter under different wind speeds

wind speed due to the different power flow distribution, including the different output of generators, ratio of transformers, shunt capacitors and DC transmission power.

Furthermore, from the Fig. 9, the DC transmission real power in rectifier P_{dr} and inverter P_{di} fluctuates in the vicinity of 1.0 and 0.97 p.u., respectively. In contrast, the reactive power consumption Q_{dr} by rectifier fluctuates greatly, which also causes the different reactive power of generators under the variational wind speeds. It can be observed from the Fig. 10, compared to the trigger angle α_i,

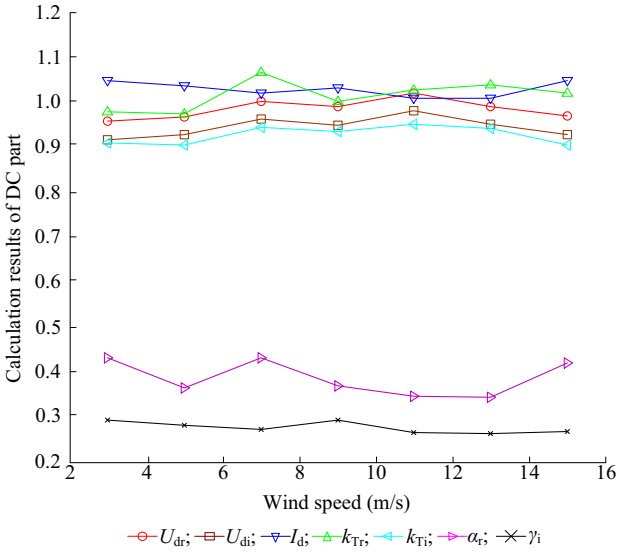

Fig. 10 Calculation results of DC part under different wind speeds

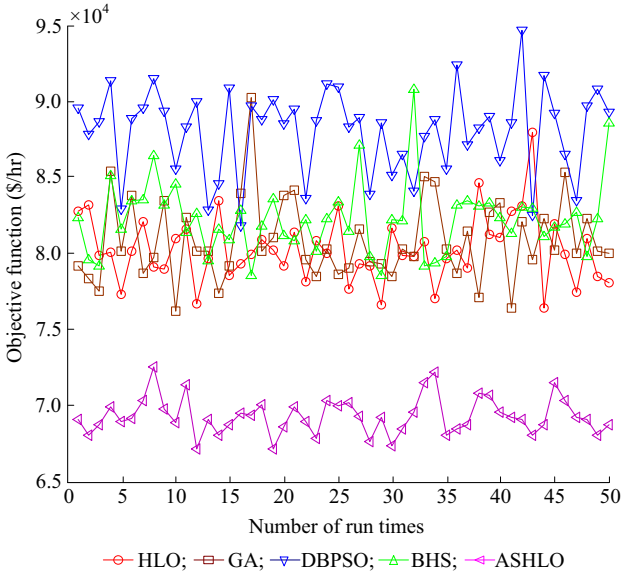

Fig. 11 Objective function of different methods under different run times

there are no significant fluctuations in other calculation results of DC part. That is mainly caused by the specified control mode as well as the coupling relationship between AC system and HVDC transmission line, based on the voltage U on the converter AC bus.

4.2 Modified IEEE 118-bus AC/DC hybrid test system

The modified IEEE 118-bus AC/DC hybrid test system originates from the IEEE 118-bus test system [22, 23], substituting DC transmission line for AC transmission line connecting nodes 30 and 38, and adding shunt capacitor on node 30. The corresponding parameters and control mode of HVDC transmission line, and the coefficients of valve-point loading effects of every six generators as well as their carbon tax coefficients, are the same as that in 4.1. Besides, the upper bound of the line currents is set three times as large as that in the original test system, and the upper bound of reactive output by some generators are also expanded due to adding one HVDC line. The penalty multiplier reset as $\lambda = 100000$ in this test system.

Firstly, no wind farms are assumed to integrate with this hybrid power system, and fifty times independent repeated experiments are carried out by ASHLO method, HLO method, GA method, DBPSO method, and BHS method. Fig. 11 shows the objective function of different methods under different run times, and Table 7 summarizes the minimum, maximum, mean, and standard deviation of the objective function by different methods during the fifty times independent repeated experiments.

It can be observed from the Table 7 and Fig. 11 that, compared to other heuristic intelligent optimization method, ASHLO method obtains the least standard deviation of the objective function, which implies that the ASHLO method has good convergent property and robustness again. Moreover, the least mean value of the objective function obtained by ASHLO method also shows its excellent feature, not easy falling into the local optima.

Table 7 Results of objective function of different methods

Method	f^{min}	f^{max}	f^{mean}	$f^{deviation}$
HLO	76495	88004	80307	2216.9
GA	76249	90302	80895	2709.9
DBPSO	81867	94727	88099	2872.7
BHS	78582	90880	82334	2405.9
ASHLO	67152	72598	69341	1227.2

Then, in order to research the impacts of locations of HVDC transmission line on the AC/DC OPF results, four

Table 8 Calculation results of DC part under different cases

Variables	U_{dr}	U_{di}	I_{dr}	I_{di}	k_{Tr}
Case1	0.9675	0.9251	1.0944	1.0944	1.0659
Case2	0.9615	0.9105	1.3143	1.3143	1.0119
Case3	0.9432	0.9018	1.0672	1.0672	1.0709
Variables	k_{Ti}	α_r	γ_i	φ_r	φ_i
Case1	1.0140	17.1900	16.3651	18.8790	18.2487
Case2	1.0372	15.3886	24.5256	17.8075	26.1670
Case3	1.0278	22.1139	16.2377	23.4225	18.1341

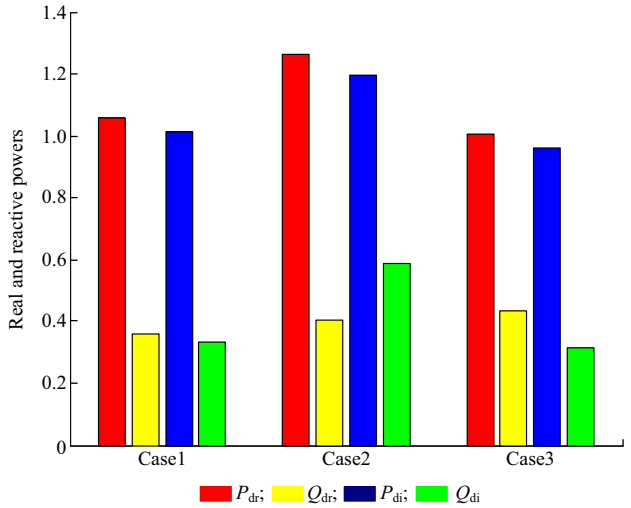

Fig. 12 Real and reactive powers of rectifier and inverter under different cases

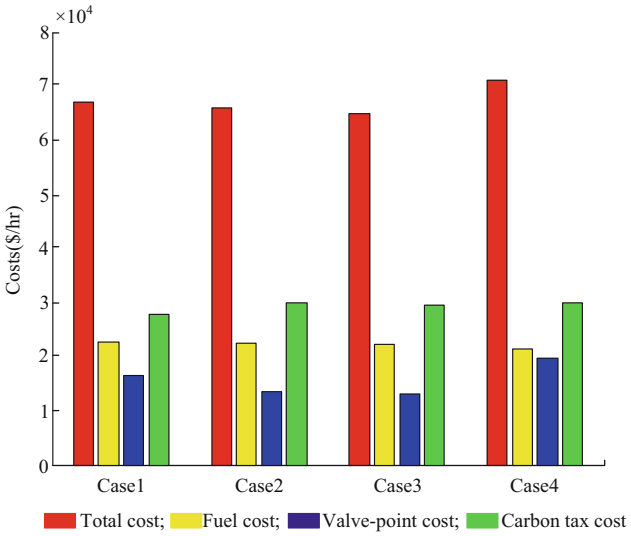

Fig. 13 Fuel cost, valve-point cost, and carbon tax cost under different cases

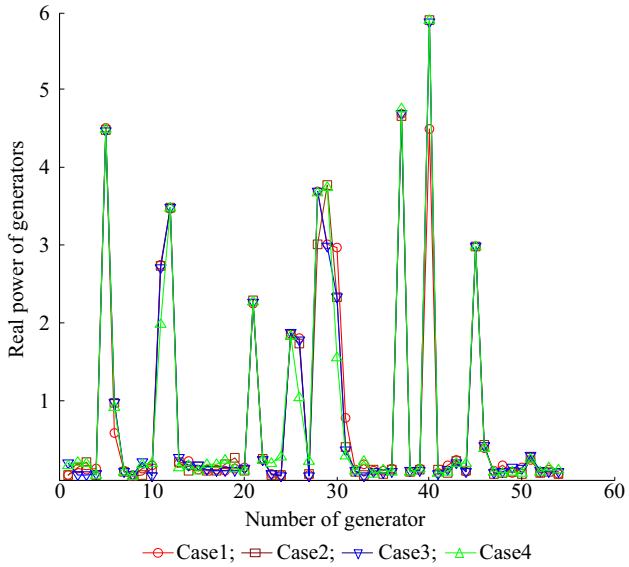

Fig. 14 Real power of generator under different cases

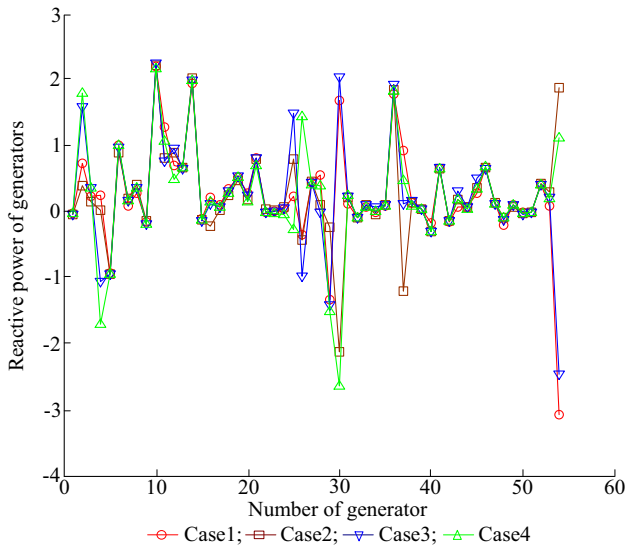

Fig. 15 Reactive power of generator under different cases

cases are considered. Case1 means the HVDC transmission line connecting nodes 30 and 38. Case2 means the HVDC transmission line connecting nodes 63 and 64. Case3 means the HVDC transmission line connecting nodes 94 and 95. Case4 means there are noHVDC transmission line adding to this modified power system. The ASHLO method is employed to solve the OPF problem under different cases. Tables 8 and Figs. 12, 13, 14, 15 and 16 give the corresponding optimal solutions, including DC variables, outputs of generators, real and reactive powers of rectifier and inverter, fuel cost, valve-point cost, carbon tax cost, amplitude of AC node voltage, respectively.

From the Table 8 and Fig. 12, according to the simple calculation, the maximal DC transmission real power in Case2 can reach 1.2637 p.u. while that only 1.0588 p.u. in Case1 and 1.0066 p.u. in Case3. What's more, it can be observed from the Figs. 13–14, although the total real power of generators, 46.1939 p.u. in Case2, is larger than that 45.9030 p.u. in Case1, 46.0223 p.u. in Case3, and 45.9133 p.u. in Case4, the total cost 65942 $/hr in Case2, is lower than that 67152 $/hr in Case1, and 71047 $/hr in Case4. That also indicates the impacts of variational locations of HVDC transmission line on the OPF results exist again. Besides, the total costs obtained by Case1, Case2 and Case3, are all less than that by Case4, which justifies the improvement of adding HVDC transmission

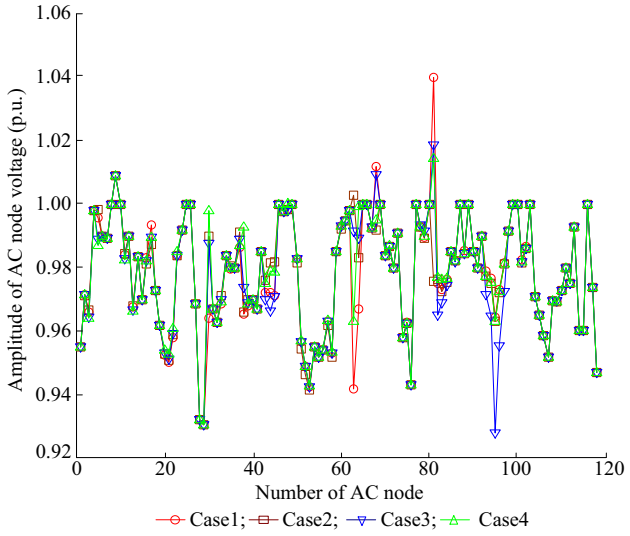

Fig. 16 Amplitude of AC node voltage under different cases

line to this modified test system over the original system standing from the economic point of view.

Meanwhile, it can be seen from the Fig. 13 that the total cost of each Case is in terms of fuel cost, valve-point cost, and carbon tax cost. Although the total cost in Case3, 64903 $/hr, is lower than that in other Cases, the carbon tax cost in Case3, 29520 $/hr, is larger than that in Case1, 27819 $/hr. The fuel cost and valve-point cost in Case3 are decreased to 22364 $/hr and 13019 $/hr, which demonstrates that the minimal total cost in Case3 is obtained at the cost of increasing carbon tax cost and decreasing fuel cost as well as valve-point cost.

From Figs. 15–16, it is clear to see that the different reactive power of generators and amplitude of AC node voltage under different Cases exist due to the variational locations of HVDC transmission line integration into the AC network and its different optimal HVDC transmission powers. Although the converters in Case2 consumes great reactive power, the total reactive power of generators in Case2, 13.5647 p.u., is lower than that in Case1, 14.2331 p.u., and Case3, 14.7018 p.u. That because a lot of shunt capacitors, 2.8716 p.u., are required for this Case, which can also compensate for lacking of reactive powers on the corresponding node and maintain the voltage level.

5 Conclusion

This paper aims at application of the adaptive simplified human learning optimization method (ASHLO) to solve AC/DC OPF problem, which takes the valve-point loading effects of generators, carbon tax, and prohibited operating zones into account. To simulate the human learning process, the random learning operator, individual learning operator, social learning operator, and adaptive strategies are involved in the proposed ASHLO method. The ASHLO method and other heuristic intelligent optimization methods are tested on the modified IEEE 30-bus and 118-bus AC/DC hybrid test system. Some important conclusions can be drawn from the simulation results.

1) Compared to the GA method, HLO method, BHS method and DBPSO method, ASHLO method has good convergent property and robustness. Escaping from the local optima is also the obvious characteristic of the ASHLO method.
2) The impacts of wind speeds on the AC/DC OPF results exist, which indicates that the wind power integration plays a positive role in reducing the total cost. Whereas, the integration of wind power will not always decrease the valve-point cost due to its function property.
3) The impacts of locations of HVDC transmission line into the AC network on the AC/DC OPF results also exist. Although the Case3 obtains the least total cost, the DC transmission power in Case3 is also minimal. Besides, the minimal total cost in Case3 is obtained at the cost of increasing carbon tax cost and decreasing fuel cost as well as valve-point cost.

Acknowledgment This work was supported by National Natural Science Foundation of China (No. 51377103), and by the technology project of State Grid Corporation of China: Research on Multi-Level Decomposition Coordination of the Pareto Set of Multi-Objective Optimization Problem in Bulk Power System (No. SGSXDKY-DWKJ2015-001). The authors greatly acknowledge the support from State Energy Smart Grid R&D Center (SHANGHAI). Besides, the authors would like to extend their sincere gratitude to Ph.D. Wei YE, from Ludwig-Maximilians-Universität München, Germany, for his instructive advice and useful materials.

References

[1] Cao J, Du WJ, Wang HF, Bu SQ (2013) Minimization of transmission loss in meshed AC/DC grids with VSC-MTDC networks. IEEE Trans Power Syst 28(3):3047–3055
[2] Rabiee A, Soroudi A, Keane A (2015) Information gap decision theory based OPF with HVDC connected wind farms. IEEE Trans Power Syst 30(6):3396–3406
[3] Saplamidis V, Wiget R, Andersson G (2015) Security constrained optimal power flow for mixed AC and multi-terminal HVDC grids. IEEE Eindhoven Power Tech, pp 1–5
[4] Li X, Cao J, Du DJ (2015) Impact evaluation of wind power integration on power system using optimal power flow tool. Trans Inst Meas Control 37(3):362–371

[5] Gu CH, Ai Q (2007) Optimal power flow calculation based on the improved interior method for a system integrated with wind farms. Electr Power 40(1):89–93
[6] Chen JF, Chen HY, Duan XZ (2006) Multi-period dynamic optimal power flow in wind power integrated system. Proc CSEE 26(3):31–35
[7] Lee F, Breipohl A (1993) Reserve constrained economic dispatch with prohibited operating zones. IEEE Trans Power Syst 8(1):246–254
[8] Li YZ (2014) Optimal power system dispatch and decision making. Ph.D. Degree Dissertation, South China University of Technology, pp 15–41
[9] Tan Y, Li CB, Cao YJ, Lee KY, Li LJ, Tang SW, Zhou L (2015) Improved group search optimization method for optimal power flow problem considering valve-point loading effects. Neurocomputing 148:229–239
[10] Li YZ, Wu QH (2013) Discussion of 'closure to discussion on 'hybrid soa-sqp algorithm for dynamic economic dispatch with valve-point effects'' S. Sivasubramani et al. Energy. Energy 55:1205–1206
[11] Alsumait J, Sykulski J, Al-Othman A (2010) A hybrid GA and SQP method to solve power system valve-point economic dispatch problems. Appl Energy 87(5):1773–1781
[12] Park JB, Jeong YW, Shin JR, Lee KY (2010) An improved particle SWARM optimization for nonconvex economic dispatch problems. IEEE Trans Power Syst 25(1):156–166
[13] Sinha N, Chakrabarti R, Chattopadhyay PK (2003) Evolutionary programming techniques for economic load dispatch. IEEE Trans Evolut Comput 7(1):83–94
[14] AlRashidi MR, El-Hawary ME (2007) Hybrid particle SWARM optimization approach for solving the discrete OPF problem considering the valve loading effects. IEEE Trans Power Syst 22(4):2030–2038
[15] Li YZ, Li MS, Wu QH (2014) Energy saving dispatch with complex constraints: prohibited zones, valve point effect and carbon tax. Int J Electr Power Energy Syst 63:657–666
[16] Huang C, Li Y, Lai XH, Li XQ (2012) Optimal cleaning power generation investiment strategy in a carbon tax and CO_2 emission trading framework. Adv Mater Res 347–353:2805–2810
[17] Wang Y, Wang C, Miller CJ, McElmurry SP, Miller SS, Rogers MM (2014) Locational marginal emissions: analysis of pollutant emission reduction through spatial management of load distribution. Appl Energy 119:141–150
[18] Wang L, Ni HQ, Yang RX, Pardalos PM, Du X, Fei MR (2015) An adaptive simplified human learning optimization algorithm. Inf Sci 320:126–139
[19] Cao J, Yan Z, Li JH, Cao L (2016) Probabilistic power flow calculation for AC/DC hybrid systems including wind farms integration. Electric Power Automation Equipment (Accepted)
[20] Yang H, Zou B (2012) A three-point estimate method for solving probabilistic power flow problems with correlated random variables. Autom Electr Power Syst 36(15):51–56
[21] Xu XY, Yan Z, Feng DH, Wang Y, Cao L (2014) Probabilistic load flow calculation based on rank correlation coefficient of input random variables. Autom Electr Power Syst 38(12):54–61. doi:10.7500/AEPS20130429008
[22] Cao J, Yan Z, Fan X, Xu XY, Li JH, Cao L (2015) AC/DC power flow computation based on improved levenberg-marquardt method. Int J Emerg Electr Power Syst 16(1):1–13
[23] Cao J, Yan Z, Xu XY (2015) A modified levenberg-marquardt approach to explore the limit operation state of ac/dc hybrid system. IEEE Power Energy Soc Gen Meet, Denver, pp 1–5
[24] Wang XF, Fang WL, Du ZC (2003) Modern power system analysis. Science Press, Beijing, pp 186–201
[25] Wang L, Yang RX, Ni HQ, Ye W, Fei MR, Pardalos PM (2015) A human learning optimization algorithm and its application to multi-dimensional knapsack problems. Appl Soft Comput 34:736–743
[26] Wang L, Ni HQ, Yang RX, Fei MR, Ye W (2014) A simple human learning optimization algorithm. Commun Comput Inf Sci 462:56–65
[27] Ye W (2013) Multi-objective node placement of large-scale industrial wireless sensor networks based on human learning optimization algorithm. Master Degree Dissertation, Shanghai University, pp 26–36

Jia CAO received the B.Sc. degree from Hunan International Economics University, major in Electrical & Information Engineering, Changsha, China, in 2010, and the M.Sc. degree from Shanghai University, major in System Engineering, Shanghai, China, in 2013, respectively. He is currently pursuing the Ph.D. degree in Shanghai Jiao Tong University, major in Electrical Engineering, Shanghai, China. His research interest is in power system optimization and probabilistic methods applied to power systems.

Zheng YAN received his B.Sc., M.Sc. and Ph.D. degrees, all in Electrical Engineering, from Shanghai Jiao Tong University in 1984, and Tsinghua University in 1987 and 1991, respectively. Before joining Electrical Engineering department of Shanghai Jiao Tong University in 2004 as a full professor, he had been on research cooperation at Ibaraki University in Japan (1994–1996), Cornell University (1997–2001), the University of Hong Kong (2001–2004). His research interests are in application of optimization theory to power systems and power markets, and dynamic security assessment.

Xiaoyuan XU received his B.Sc. and Ph.D. degrees from the department of electrical engineering, Shanghai Jiao Tong University, Shanghai, China, in June 2010 and June 2016, respectively. His research interests include probabilistic load flow and power system optimization.

Guangyu HE received his B.Sc. degree in automation and Ph.D. degree in electrical engineering from Tsinghua University, Beijing, China, in 1994 and 1999, respectively. He is currently a full professor of the department of electrical engineering, Shanghai Jiao Tong University. His research interests are in the field of power system analysis and operations, and linear and nonlinear optimization for large-scale problems.

Shaowei HUANG received his B.Sc. and Ph.D. degrees from the department of electrical engineering, Tsinghua University, Beijing, China, in July 2006 and June 2011, respectively. His research interests are parallel and distributed computing and their applications in power systems.